Influences of changing sea ice and snow thicknesses on simulated Arctic winter heat fluxes

Laura Landrum[1], Marika M Holland[1]

[1]National Center for Atmospheric Research, Boulder, CO, USA

Correspondence to: Laura Landrum (landrum@ucar.edu)

Abstract. In the high latitude Arctic, wintertime sea ice and snow insulate the relatively warmer ocean from the colder atmosphere. While the climate warms, wintertime Arctic surface heat fluxes remain dominated by the insulating effects of snow and sea-ice covering the ocean until the sea ice thins enough or sea ice concentrations decrease enough to allow for direct ocean-atmosphere heat fluxes. The Community Earth System Model Large Ensemble (CESM1-LE) simulates increases in wintertime conductive heat fluxes in the ice-covered Arctic Ocean by ~7-11 W m^{-2} by mid-21st century, thereby driving an increased warming of the atmosphere. These increased fluxes are due to both thinning sea ice and decreasing snow on sea ice. The simulations analyzed here use a subgridscale ice thickness distribution. Surface heat flux estimates calculated using grid-cell mean values of sea ice thicknesses underestimate mean heat fluxes by ~16-35% and overestimate changes in conductive heat fluxes by up to ~36% in the wintertime Arctic basin even when sea ice concentrations remain above 95%. These results highlight how wintertime conductive heat fluxes will increase in a warming world even during times when sea ice concentrations remain high, and that snow and the distribution of snow play significantly impact large-scale calculations of wintertime surface heat budgets in the Arctic.

1 Introduction

The Arctic is warming rapidly, and much more rapidly than lower latitudes. This Arctic amplification (AA) is due to a combination of a number of related mechanisms, including sea ice loss, lapse rate and Plank feedbacks, and changing water vapor and clouds, among others (e.g. Graverson and Wang, 2009; Kumar et al, 2010; Screen et al., 2013; Pithan and Mauritsen, 2014; Vavrus, 2004; Feldl et al., 2020). Sea ice loss contributes to increased surface warming through two primary methods: an albedo feedback, and an insulating effect. The albedo feedback results from sea ice concentration losses that expose dark ocean water and sea ice surface state changes, including reduced snow cover and increased ponding, that darken the ice surface. These decrease the surface albedo and increase surface absorption of incoming radiation. The insulating effect results from thinning of the sea ice and overlying snow: in the winter, sea ice and snow insulate the relatively warmer ocean from the colder atmosphere. As sea ice and snow thin, more heat can be conducted through the sea ice to the atmosphere, influencing the ice-atmosphere exchange. Thinning ice and snow and increasing conductive heat fluxes can also lead to increased basal sea ice growth – a feedback in a warming world that is seen temporarily in climate projections before warming temperatures overwhelm this feedback and ice growth declines (e.g. Petty et al., 2018; Keen et al, 2020).

A large body of previous research has investigated the interactions between sea ice loss and AA. Most of the published research and the majority of the ongoing Polar Amplification Model Intercomparison Project (PAMIP) experiments focus on the influence of changes in sea ice concentration (SIC) on Arctic warming (e.g. Peings & Magnusdottir, 2014; Sun et al., 2015; Smith et al., 2019; Sun et al., 2015). Less attention has been paid to the influence of winter sea ice thinning on Arctic surface warming, in part because observations of sea ice thickness (SIT) have only recently become more readily available, and in part because the effects of SIC losses tend to be large compared to those from SIT changes. Although wintertime SIC in the central Arctic remain high and have changed very little over the satellite era, the sea ice has thinned dramatically (e.g. Kwok and Rothrock, 2009; Kwok, 2018). Sea ice volume has decreased by roughly 66% since submarines have been measuring (1958-1976) – and by 50% since 1999 (Kwok, 2018; Lindsay and Schweiger, 2015).

Recent work with atmosphere-only models over both the historical time period and future scenarios suggest that the atmospheric response to SIT changes are strongest in the cold season and at the surface, with atmospheric responses to SIT changes of similar or smaller magnitudes than the responses to SIC changes (e.g. Gerdes, 2006; Krinner, 2010; Lang et al., 2017; Labe et al., 2018b; Sun et al., 2017). There is qualitative agreement that the inclusion of SIT changes along with SIC changes lead to an enhancement of surface AA, although the range across different studies is large: two studies focused on late 20th-early 21st century found annual AA enhanced by ~37-50% with the inclusion of SIT changes (Lang et al., 2018; Sun et al., 2017), whereas AA increased by ~10% in the future simulations (2051-2080) of Labe et al. (2018b).

Our understanding of the influence of SIT on winter surface AA is further complicated by the presence of snow on sea ice, as well as the heterogeneous distribution of both snow and sea ice thicknesses. Snow is a more effective insulator than sea ice – and relatively small changes in snow thicknesses can result in large changes in conductive heat fluxes through the ice with consequent impacts on ice-atmosphere exchange. To our knowledge, there have been relatively few basin-scale studies on the effects of snow-on-sea-ice on the winter surface heat budgets in the Arctic in a changing climate. Previous work investigating SIT changes on winter Arctic warming have not typically considered the effects of changing snow cover and often exclude this in the experimental design. For example, Lang et al., (2018) used atmosphere only models that do not allow snow to accumulate on sea ice. Furthermore, previous work with atmosphere-only models specifies grid-cell averaged values for SIT, thus calculating conductive fluxes (which are inversely related to sea ice and snow thicknesses) from an average SIT rather than as a sum over a sub-gridscale thickness distribution. This introduces errors relative to fully-coupled model simulations which typically include a treatment of subgridscale ice thickness variations. These sources of errors and uncertainties also apply to global reanalysis products, most of which use constant sea ice thicknesses and no snow on sea ice for their product estimates (e.g. Wang et al., 2019) and show particularly large errors over the Arctic Ocean (e.g. Bromwich et al., 2018; Jakobson et al., 2012 and references therein). In particular, the lack of snow on sea ice in reanalysis products and the influence on the conductive heat flux results in a warm bias relative to observations (Batrak and Müller, 2019)

In this study we investigate the influence of SIT, snow thickness and heterogeneity in these fields on the Arctic winter energy budget in the climate modeling environment. We explore how projected thickness changes in both sea ice and snow influence conductive heat fluxes and ice-atmosphere heat exchange. We further investigate the importance of heterogeneity in sea ice and snow thicknesses at a model sub-gridcell level, how this impacts conductive heat flux calculations, and quantify the errors that are introduced by using grid-cell average SITs rather than heterogeneous fields. We explore how the wintertime Arctic heat fluxes change during a time period (1950-2070) when winter Arctic basin SICs remain high while ice and snow show dramatic thinning. This allows us to elucidate the dynamic nature of the influence of sea ice and snow thicknesses on surface heat budget even when SIC changes are small. To set context, we also compare results from the wintertime high latitude Arctic to other seasons (fall) and regions that are undergoing rapidly changing SIC and associated changes in surface heat fluxes due to open water formation.

2 Models and Analysis

2.1 CESM1-LE

We use the Community Earth System Model version 1 Large Ensemble (CESM1-LE; Kay et al., 2015) to explore relationships between Arctic wintertime conductive heat fluxes and sea ice and snow thickness fields. The CESM1-LE consists of 40 simulations forced with historical forcing from 1920-2005, and then the Representative Concentration Pathway 8.5 (RCP8.5) forcing from 2005-2100 (the no-mitigation scenario with a top of the atmosphere radiative forcing of 8.5 W/m^2 by 2100; Meinshausen et al., 2011). The sea ice model component (CICE; Hunke et al., 2015) in the CESM1 uses a sub-gridscale ice thickness distribution (ITD) in which thermodynamics are calculated over 5 discrete sub-gridcell thickness categories with minimum thicknesses of 0., 0.64, 1.39, 2.47 and 4.57 meters. The presence of the ITD influences both the mean climate state and climate feedbacks (Holland et al., 2006). The simulated ITD and sea ice concentrations within each category evolve through ice growth and melt, ridging due to mechanical forcing, and ice transport (e.g. Thorndike et al., 1975). The resulting concentrations of sea ice can range from 0 to 100% (although values of 100% are rare due to lead formation) in the discrete thickness layers. Snowfall can accumulate on sea ice and be affected by snow melt, ice ridging and transport. Effectively this means that a different snow depth is present across the different ice thickness categories. Ice-atmosphere fluxes are calculated separately in each sea ice thickness category, weighted by the concentration in each category, and passed as grid-cell means to the flux coupler for use in the atmospheric model. CICE uses a multi-layer thermodynamic scheme (Bitz and Lipscomb, 1999; "BL99") that includes the effects of a prescribed vertical salinity profile. Comparisons with the Pan-Arctic Ice Ocean modelling and Assimilation system (PIOMAS; Zhang & Rothrock, 2003) sea ice thickness reanalysis product show that the CESM1-LE and PIOMAS agree well for both summer and winter rates of sea ice volume change (Labe et al., 2018a). CESM1-LE and PIOMAS also tend to agree on regional mean thicknesses and variabilities throughout much of the Arctic with the

exception of the Canadian Archipelago and coastal Greenland, where the CESM1-LE overestimates sea ice volumes compared to PIOMAS (and PIOMAS underestimates volumes compared to buoy and submarine data).

2.2 0-layer thermodynamic conductive heat-flux model

Not all thermodynamic variables for individual ice thickness categories were saved as part of the CESM1-LE output. In order to disentangle the relative influences of sea ice and snow thicknesses and their distributions, we use the available CESM1output along with the 0-layer thermodynamic model of Semtner (1976) to estimate the conductive heat flux. This simple 0-layer model – developed originally to minimize computational costs associated with ice thickness calculations in climate models – assumes a linear temperature gradient through the sea ice and snow, and that the conductive heat flux through the ice+snow layer is:

$$F_{cond} = \frac{K_s(T_b - T_s)}{h_s + K_s\left(\frac{SIT}{K_i}\right)} \quad \text{Eq. 1}$$

where

K_s, K_i = snow and ice conductivities of heat (0.3 $Wm^{-1}degK^{-1}$, 2.0 $Wm^{-1}degK^{-1}$)

h_s, SIT = snow and ice thicknesses

T_b ,T_s = temperatures at the bottom (ocean-ice) and surface (ice-atmosphere) of the ice

The conductive heat flux reduces to:

$$F_{cond} = \frac{K_i \Delta T}{h_{eff}} \quad \text{Eq. 2}$$

where

$\Delta T = T_b - T_s$

$h_{eff} = (SIT + (K_{ratio} * h_s))$ is a measure of the effective thickness from an insulating perspective, with

$K_{ratio} = K_i/K_s$

In the Arctic winter, surface temperatures are cold - well below the melting point of ice and snow - and the net surface energy budget (the sum of the net short- and longwave radiation, and sensible and latent heat fluxes) in ice covered regions is balanced

by the conductive heat flux from the ocean through the sea-ice and snow. Where open water is present, such as leads in the sea ice, direct atmosphere-ocean exchange also occurs. Climate simulations that prescribe constant sea ice thickness such as those used in Atmospheric Model Intercomparison Project (AMIP) and most of the Polar Amplification Model Intercomparison Project (PAMIP; Smith et al., 2019) experiments only allow for changes in conductive heat fluxes to occur through changes in temperatures and possibly through snow depth changes resulting from changing snowfall. This results in inaccurate estimates for changes in surface heat fluxes (and thus also temperatures) which can be quite sizable and of the wrong sign. For example, in response to 20°C surface warming, changes in conductive heat fluxes from a "typical" 20th Century mid-Arctic ocean (with 2.0 m thick ice covered by 0.1 m thick snow with a surface to base ΔT of 40°C) will be roughly halved if SIT and snow thicknesses are held constant but doubled if the ice thins to 0.5m with 0.02 m of snow (e.g. Table 1). In CESM2 PAMIP (100 member ensembles comparing present-day and future changes from 1850s; Smith et al., 2019; Sun et al., 2022) and AMIP (10-member ensembles investigating historical changes; Hurrell et al., 2008; Simpson et al., 2020) simulations in which ice thickness is prescribed and unchanging, net surface heat fluxes increase outside of sea ice covered areas but decrease over sea ice covered areas as the surface temperatures warm (Figure 1). For reference, Arctic sea ice volume decreased by ~66% from the mid-twentieth century to the present (Kwok, 2018; Lindsay and Schweiger, 2015). Thus, keeping SIT constant during this period, in direct contrast to observations, artificially introduces errors in surface heat flux calculations – and thus also temperature changes over sea ice covered regions. These differences in wintertime conductive heat fluxes are not insignificant contributions to the surface energy budget (e.g., Huwald et al., 2005). Notably, many simulations that have been used to diagnose Arctic Amplification rely on AMIP-type simulations which specify the fractions of open water and sea ice yet neglect ice thickness changes (e.g. Smith et al., 2019). Even when ice thickness anomalies are applied (e.g. Lang et al.2017; Labe et al. 2018b; Sun et al., 2017; Smith et al., 2019), they are specified for a mean gridcell value, missing the potential role of ice thickness heterogeneity which could be important given that the conductive flux has a non-linear dependence on ice and snow thickness. AMIP and PAMIP protocols do not specify snow depths as part of the sea ice boundary conditions and different modelling systems use different approaches to modifying (or not) the snow over sea ice in perturbed climate simulations.

2.3 Analysis

We are interested in wintertime Arctic heat fluxes during a period when wintertime central Arctic SIC remain relatively high and changing sea ice and snow thickness will play a dominant role in changing surface fluxes. Thus, we focus initially on 1950-2070 and on the month of February to explore in detail relationships between conductive heat fluxes, snow and sea ice thicknesses, and thickness distributions. Timeseries presented are area averages over the Arctic Ocean (68°-90°N from 100°-243°E, and 80°-90°N elsewhere – see inset in Figure 2b), thereby reducing the influence of changes in winter sea ice concentrations (SIC) that are seen in the simulations during this time period in the neighboring regions. Changes in conductive heat fluxes due to thinning sea ice dominate the surface heat budget until the sea ice thins enough to subsequently start retreating, exposing open ocean. To highlight this contrast between ice covered regions and time periods, and those with increasing open water areas, we also show timeseries from the Kara and Barents seas (see inset in Figure 5) and some results

from October when SIC are already changing rapidly at the beginning of the 21st Century. Our regional definitions are those used by the National Snow & Ice Data Center (www.nsidc.org) and discussed in Parkinson and Cavalieri (2012), Cavalieri and Parkinson (2008), and Parkinson et al. (1999).

We then explore the relative and changing importance of sea ice conductive heat fluxes to the total surface heat fluxes in a warming world in the cold season (October through March) in the 21st century. In the high-latitude Arctic winter, when there is no solar radiation and the surface air temperature is well below the freezing point, the net surface heat flux over the sea ice (total surface short- and longwave radiation, and sensible and latent heat fluxes) is balanced by the conductive heat flux through the ice and snow. In regions not 100% covered by sea ice, there will also be heat flux from the ocean to the atmosphere. The relative contributions of heat fluxes from ocean and sea ice areas will change both as ice and snow thin, and as sea ice concentrations decrease. We ask how these relative contributions change in winter months as the projected climate warms and compare ice-covered regions with two regions (Barents Sea and Kara Sea) that are experiencing significant wintertime sea ice concentration losses from 2010-2070.

We also assess the role of sub-gridcell sea ice thickness distributions in simulated conductive heat fluxes. Model output of conductive heat flux is available on a gridcell level and is computed as the area weighted average of the sub-gridcell conductive heat fluxes. This explicitly accounts for changing ice and snow thicknesses, surface temperatures, and areal concentrations for the different ice thickness categories. Although sub-gridcell conductive heat flux information that would enable us to directly relate changes in the sub-gridcell ITD to the net flux was not saved and is not available, sub-gridcell ice and snow thicknesses are available. Comparisons between the model net gridcell conductive heat fluxes to those calculated using the sub-gridcell ice and snow thicknesses, the gridcell surface temperatures and the 0-layer model demonstrate that the 0-layer model gives a good approximation for this analysis (Supplemental material). We then compare the model conductive heat fluxes which account for the subgridscale ice thickness distribution (CESM1-LE) with those calculated from the gridcell mean SIT and snow thicknesses using the 0-layer model ("MNthick") to investigate the influence of snow and sea ice heterogeneity on conductive heat flux calculations.

3 Results

3.1 Sea ice and snow thicknesses

Over the Arctic Ocean, simulated February surface temperatures and conductive heat fluxes, which are equivalent to the ice-atmosphere heat exchange, increase by ~8°C and 9 W/m^2 between the late 20th century and 2070 in the CESM1-LE (Figure 2a). The turbulent heat flux exchange between the ocean and the sea ice increases during this time as well – however by less than 1 W/m^2 and therefore is not a dominant contribution to the increased net surface heat exchange. Increases in conductive heat flux are driven by decreases in sea ice and snow thickness, since the increase in surface temperatures alone would result

in a decrease in conductive heat fluxes (Equation 2). During this time, sea ice concentrations in the Arctic Ocean remain high yet sea ice and snow thin dramatically (Figure 2b), with a mean total effective thickness (h_{eff}) decreasing from a peak near 6 m in the 1970s to 1.5 m by 2070 (Figure 2c). Snow thicknesses averaged over the Arctic Ocean region are typically less than 0.5 m thick – much thinner than sea ice - however snow, and changes in snow, make significant contributions to both the total effective thickness and the changes in total effective thickness, due to the much larger insulating capacity of snow (Figure 2c). The decreasing wintertime snow depths over the 21st Century in the CESM1-LE are due primarily to sea ice forming later in the fall, which in turns leads to a later start of accumulation of snow on the sea ice (e.g. Webster et al. 2014; Webster et al. 2018; Webster et al., 2020). This mechanism has also been found in projections of snow on sea ice (Hezel et al., 2012) and in observations (Webster et al. 2014; Webster et al. 2018). In addition, as the temperatures warm, the rain/snow seasons increase/decrease (e.g. Webster et al., 2020).

Conductive heat fluxes increase first over the East Siberian and Chukchi seas (Figure 3). By the 2050s, increases in conductive heat fluxes of 9-12 W/m^2 are seen not only in the Chukchi and East Siberian seas, but also extending into the Beaufort Sea and the Central Arctic Ocean. Surface temperature increases likewise show the earliest and greatest increases on the Pacific side of the Arctic Ocean. However, by the 2050s the areas of greatest warming (>10°C) are present over comparatively larger sections of the Arctic Ocean, Beaufort Sea and extend as far as northern Greenland. Sea ice concentrations remain above 95% in the Arctic ocean even by the 2050s. As such, changes in heat fluxes from the relatively warmer surface to the colder atmosphere primarily result from thinning sea ice and snow rather than increases in open water (see section 3.2). Changes in sea ice thicknesses in the CESM1-LE tend to be largest from the Canadian Archipelago, across the Central Arctic ocean and on to the East Siberian sea (Supplemental material), whereas changes in snow thickness are greatest near the Canadian Archipelago and northern and eastern Greenland. Changes in both sea ice and snow thicknesses are important contributors to the changes in effective thickness (Figure 3). Although snow depth changes are small compared to changes in SIT, they contribute 40% or more to the changes in effective thicknesses from the central Arctic Ocean to the Canadian Archipelago, Greenland and into the Atlantic sector of the Arctic ocean (Figure 3 and Supplemental material). It is important to note that changes in conductive heat fluxes during this time are mitigated by changes in surface temperatures: the roughly 13° surface warming over this period would lead to ~5 W/m^2 *decrease* in conductive heat flux if the sea ice and snow did not thin (and as they do in the AMIP and PAMIP atmosphere only runs when SITs are held constant - e.g., Figure 1).

3.2 Relative contributions of conductive heat flux changes to total surface heat flux changes in a warming climate

Changes in conductive heat fluxes due to thinning sea ice dominate the surface heat budget until the sea ice thins enough to subsequently start retreating, whereupon the surface heat flux quickly becomes dominated by fluxes from exposed open water (Figures 4 and 5). Ensemble mean February net surface heat fluxes over the Arctic ocean increase modestly from the 1950s to the 2010s (~3-6 W/m^2), then by ~10-18 W/m^2 by the 2050s. Arctic ocean SICS remain above 98% - increases in surface heat flux are primarily due to changes in snow and ice thicknesses, with open water areas contributing less than 10-25% to the net surface heat flux budget. In contrast, outside of the ice covered areas, increases in surface heat fluxes are larger than 25 W/m^2

and predominantly due to fluxes from open water. In February, these areas expand from the Sea of Okhotsk and the Bering, Kara and Barents seas in the 2010s to include most of the Arctic ocean by the end of the 21st Century. Rates of surface temperature warming reflect this as well – with the highest February Arctic Amplifications occurring initially over the Chukchi and East Siberian Seas, where sea ice is thinning, over the Barents and Kara Seas by the 2050s, and finally over large sections of the Arctic Ocean as SICs fall by the 2090s (Figure 4). These patterns of relative contributions of sea ice and ocean to the net surface heat fluxes, and corresponding rates of AA, are also seen in the fall (October; Supplementary material), when observed AAs are highest (e.g. Chung et al., 2021) and underscore the transient and seasonal nature of AA which may increase in regions experiencing sea ice loss before decreasing again after becoming ice-free (e.g. Holland & Landrum, 2021). Regionally averaged timeseries show how contributions from open ocean water to the net surface heat fluxes tend to be greater than those from ice once SICs fall below ~90% - highlighting how changes in surface heat fluxes will be dominated by those over sea ice (due to thinning sea ice and snow) until sea ice itself starts retreating (Figure 5). Variability in heat fluxes from the ocean tend to be very high compared to those from sea ice, particularly in the Barents and Kara Seas.

3.3 Sea ice and snow thickness distributions

Given the nonlinear response of the conductive heat flux to ice and snow thickness, the changing distribution of ice at the sub-gridcell level may play an important role. We investigate the influence of thickness distributions on conductive heat fluxes by calculating conductive heat fluxes using the Semtner 0-layer model, daily mean sea ice and snow thicknesses over the ice-covered areas in each grid cell along with daily gridcell average surface temperatures ("MNthick"), and then averaging over the month of February. Relative to an estimate of the fluxes computed by the full model (CESM1-LE), the MNthick conductive heat fluxes underestimate heat fluxes throughout the Arctic Ocean (Figure 6a, and Supplemental material). Ensemble mean Arctic Ocean average conductive heat flux is underestimated by ~6-9 W/m^2 using MNthick (Figure 6). This highlights the importance of resolving thin ice and snow within the subgridscale ice thickness distribution.

Differences between these winter-time conductive heat fluxes throughout the Arctic basin are larger in the beginning of the 21st century (by ~35%) when considerable thick ice is present. Discrepancies between MNthick conductive heat flux estimates and CESM1-LE are reduced by the 2070s (to ~16%) when almost all the February sea ice in the Arctic Ocean has thinned considerably to less than 1m over the Arctic ocean and the ITD lies within the two thinnest sea ice categories (Figure 6b). Although grid-cell average thicknesses lead to an underestimation of mean conductive heat fluxes, they result in an overestimation in the changes in conductive heat fluxes (by ~ 36% by 2070; Figure 6a) and thus influence feedbacks in the warming climate.

4 Discussion and Conclusions

This analysis has important implications for atmosphere-only simulations and reanalysis products that require specified sea ice concentrations, sea ice thicknesses and snow depths for boundary conditions. These simulations typically prescribe changes in sea ice concentration but neglect changes in ice and snow thickness. The sea ice concentration changes lead to large changes in surface albedos and direct ocean-atmosphere heat fluxes as more ocean water is exposed to the atmosphere. However, by neglecting changes in ice and snow thickness, the changing insulating effect of sea ice is missing. As the climate warms, changing winter Arctic surface heat fluxes will be dominated by this insulating effect and resulting changes in conductive heat fluxes until the SICs decrease enough such that direct ocean-atmosphere heat fluxes become more important. In the CESM1-LE, with changing subgridscale ice and snow thicknesses, conductive heat fluxes contribute over half of the Dec-Mar surface heat fluxes until 2050-2070 (not shown). Atmosphere only simulations that consider only changes in sea ice concentrations and ignore changes in sea ice and snow thicknesses simulate decreasing conductive heat fluxes – the winter atmosphere in high SIC regions gains *less* heat from the surface under climate warming. When changing ice thicknesses and snow depths are accounted for, conductive heat fluxes increase and the atmosphere gains **more** heat from the surface. In the CESM1-LE, Arctic basin conductive heat flux increases by ~8-10 W/m^2 from 2000 to 2070 as winter SIC remain above 95%.

Sea ice and snow exhibit high spatial heterogeneity and climate models often account for this through the inclusion of a subgridscale ice thickness distribution within their sea ice treatment. This heterogeneity of both sea ice and snow fields impacts conductive heat fluxes and thus the projected changes in the net surface heat flux. Whereas most climate models participating in the most recent Coupled Model Intercomparison Project (CMIP6) employ sea ice models with sub grid-scale sea ice thickness distributions (e.g. Keen et al., 2021), atmosphere-only simulations (for example AMIP and PAMIP style simulations) calculate sea ice thermodynamics over only gridcell mean sea ice and snow thicknesses. This will underestimate mean wintertime conductive heat fluxes and, in the PAMIP simulations that allow thickness to change, will overestimate changes in conductive heat fluxes as the ice thins. These differences can be significant – in the CESM1-LE mean conductive heat fluxes calculated using grid-cell mean thicknesses lead to an underestimation of ~16-35% in mean values and an overestimation of up to ~36% in the changes in conductive heat fluxes in the wintertime Arctic basin where SIC remain above 95%.

Snow is a much more effective insulator than sea ice and plays important roles in sea ice mass budgets and climate feedbacks. Snow distributions on sea ice remain, however, an area of large uncertainty and potential errors in both climate model simulations and reanalysis products. PAMIP protocols and reanalysis products use either very simplified snow (accumulations only through precipitation) or non-existent snow routines, with resultant flux estimates that show large wintertime heat flux biases when compared to the recent Norwegian young sea-ICE campaign (N-ICE2015) observations (e.g. Bromwich et al., 2018; Graham et al., 2017). Yet snow – highly reflective and highly insulating - plays an outsized role in Arctic heat budgets. Reanalysis products show consistent warm bias in winter sea ice surface temperatures (e.g. Batrak & Muller, 2019; Graham

et al., 2017; Graham et al., 2019; Jakobson et al., 2012; Lindsay et al., 2014), with recent work attributing this to misrepresentation of snow on sea ice (Batrak & Müller, 2019).

Snow and sea ice thicknesses and distributions in the CESM1-LE are roughly equally important contributors to wintertime conductive heat fluxes. Snow depth distributions in the CESM1-LE show similar patterns compared to observations across the Arctic Basin, although simulated snow depths tend to be more evenly distributed and thicker than observed (Webster et al., 2020). Snow thicknesses in the most recent version of CESM – the CESM2 – tend to be underestimated and have low variability compared to observations. These differences between simulations are due largely to differences in precipitation and the mean sea ice state in these two models (Webster, et al., 2020). Discrepancies between simulations and observations, however, are not well understood and suggest that future collaborative work to test and improve snow distributions in the modeling environment would be important for increasing our understanding of Arctic climate and predicting snow impacts in a warming climate.

The results presented here are from a large ensemble of simulations from one climate model. Recent contributions from multiple modelling centers to the CMIP6 suggest that the sea ice components in climate models are responding consistently to external forcing (e.g. Keen et al, 2021) and our results are not expected to change fundamentally with different climate models although the timing may differ based on the mean ice state. In the CESM1-LE SICs remain above 98% in the high latitude Arctic Ocean until the end of the 21st Century and this timing will differ depending on the initial mean ice state and transient response in a given model. For example, the most recent version of the model, the CESM2 includes many changes all model components, and Arctic sea ice in the CESM2 tends to be thinner, less extensive and less persistent than in the CESM1-LE (DeRepentigny et al., 2020).

These results highlight the transient nature of the influences of SIT, snow thicknesses, and their distributions on Arctic wintertime surface heat budgets. The thermodynamics of sea ice are dependent on the mean ice state (e.g. Massonnet et al., 2018) – and this has important implications not only for sea ice evolution in a changing world, but also surface heat fluxes in ice covered areas. Models with a relatively thin sea ice mean state will have higher errors in changes in surface heat fluxes depending on whether they use grid-cell mean SITs or heterogeneous fields. Sea ice and snow on sea ice are important components of polar climate thermodynamics and their dynamic and heterogeneous nature – although complicated – play important roles in surface heat budgets.

Code and Data availability

All analysis and figures were completed using the NCAR Command Language (The NCAR Command Language v.6.6.2 (UCAR, NCAR, CISL and TDD,2019); https://doi.org/10.5065/D6WD3XH5). The scripts used to perform the analysis and

generate the figures in this manuscript are available on GitHub (https://github/llandrum/Cryosphere_SeaIce_Snow_Thicknesses_ArcticHeatFlux) and archived in Zenodo (Landrum, 2021). The CESM-LE data are freely available from the following link: http://www.cesm.ucar.edu/projects/community-projects/LENS/ (last access: 7 April 2020, Deser and Kay, 2020; Kay et al., 2015).

Author contribution

LL and MMH formulated the research goals and questions. LL made the figures and performed the analysis with input from MMH. LL prepared the manuscript with contributions from MMH.

Competing interests

The authors declare that they have no conflict of interest.

Acknowledgments

We acknowledge funding from NSF-OPP 1724748. We also acknowledge the CESM Large Ensemble Community Project and supercomputing resources (doi:10.5065/D6RX99HX) provided by the Climate Simulation Laboratory at NCAR's Computational and Information Systems Laboratory, sponsored by the National Science Foundation and other agencies.

We thank Alice DuVivier for providing the daily CESM1-TS data so that we could compare 0-layer to multi-layer model estimates of conductive heat fluxes

References

Bailey, D. A., Holland, M. M., DuVivier, A. K., Hunke, E. C., and Turner, A. K.: Impact of a New Sea Ice Thermodynamic Formulation in the CESM2 sea ice component, J. Adv. Model. Earth Sy., 12, e2020MS002154, https://doi.org/10.1029/2020MS002154, 2020.

Batrak, Y., & M. Müller. On the warm bias in atmospheric reanalyses induced by the missing snow over Arctic sea-ice. *Nat Commun* **10,** 4170 (2019). https://doi.org/10.1038/s41467-019-11975-3

Bromwich, D. A., and Coauthors, 2018: The Arctic System Reanalysis, version 2. Bull. Amer. Meteor. Soc., 99, 805–828, https://doi.org/10.1175/BAMS-D-16-0215.1.

Bitz, C. M. and Lipscomb, W. H.: An energy-conserving thermodynamic sea ice model for climate study. *J. Geophys. Res.-Oceans*, **104(C7)**. 15,669-15,677, https://doi.org/10.1029/1999JC900100, 1999.

Bromwich, D., and Coauthors: The Arctic System Reanalysis, version 2. *Bull. Amer. Meteor. Soc.*, **99**, 805–828, https://doi.org/10.1175/BAMS-D-16-0215.1, 2018.

Cavalieri, D. J., and C. L. Parkinson. Arctic sea ice variability and trends, 1979-2010, The *Cryosphere*, **6**, 881-889, doi:10.5194/tc-6-881-2012, 2012.

Cavalieri, D. J., and C. L. Parkinson. Antarctic Sea Ice Variability and Trends, 1979–2006. *J. Geophys. Res.* **113** (C07004). doi:10.1029/2007JC004564, 2008.

Chung, E., Ha, K., Timmermann, A., Stuecker, M., Bodai, T., & Lee, S. Cold-season Arctic Amplification driven by Arctic Ocean-mediated seasonal energy transfer. *Earth's Future*, 9, e2020EF001898. https://doi-org.cuucar.idm.oclc.org/10.1029/2020EF001898, 2021.

Dai, A., Luo, D., Song, M. and Liu, J.: Arctic amplification is caused by sea-ice loss under increasing CO_2. *Nat Commun* **10,** 121. https://doi.org/10.1038/s41467-018-07954-9, 2019.

DeRepentigny, P., Jahn, A., Holland, M. M., & Smith, A.: Arctic sea ice in two configurations of the Community Earth System Model Version 2 (CESM2) during the 20th and 21st centuries. *Journal of Geophysical Research: Oceans*. https://doi.org/10.1029/2020JC016133, 2020.

Deser, C. and Kay, J. E.: CESM Large Ensemble Community Project, available at: http://www.cesm.ucar.edu/projects/community-projects/LENS/, last access: 7 April, 2020.

European Centre for Medium-Range Weather Forecasts (ECMWF): IFS documentation–CY41R2. part IV: physical processes, doi: 10.21957/tr5rv27xu [Available at https://www.ecmwf.int/en/elibrary/16648-ifs-documentation-cy41r2-part-iv-physical-processes, accessed 03.29.2021.], 2016.

Feldl, N., Po-Chedley, S., Singh, H. K. A., Hay, S., and Kushner, P. J.: Sea ice and atmospheric circulation shape the high-latitude lapse rate feedback, *Nature Partner Jounals Climate and Atmospheric Science*, 3, 41, doi.org/10.1038/s41612-020-00146-7, 2020.

Gates, W. L., Boyle, J., Covey, C., Dease, C., Doutriaux, C., Drach, R., Fiorino, M., Gleckler, P., Hnilo, J., Marlais, S., Phillips, T., Potter, G., Santer, B., Sperber, K., Taylor, K. and Williams, D.: An Overview of the Results of the Atmospheric Model Intercomparison Project (AMIP I). *Bull. Amer. Meteor. Soc.*, **73**, 1962-1970 (1998).

Gerdes, R.: Atmospheric response to changes in Arctic sea ice thickness. *Geophysical Research Letters*, *33*, L18709. https://doi.org/10.1029/2006GL027146, 2006.

Graham, R. M., and Coauthors: A comparison of the two Arctic atmospheric winter states observed during N-ICE2015 and SHEBA. *J. Geophys. Res. Atmos.*, **122**, 5716–5737, https://doi.org/10.1002/2016JD025475, 2017.

Graham, Robert M., Lana Cohen, Nicole Ritzhaupt, Benjamin Segger, Rune R. Graverson, Annette Rinke, Van P. Walden, Mats A. Granskog, and Stephen R. Hudson: Evaluation of Six Atmospheric Reanalysis over Arctic Sea Ice from Winter to Early Summer. Journal of Climate, 32 (14), pp 4121-4143, https://doi.org/10.1175/JCLI-D-18-0643.1, 2019

Graversen, R. G. and Wang, M.: Polar amplification in a coupled climate model with locked albedo, *Clim. Dynam*., **33**, 629–643, 2009.

Hall, A.: The role of surface albedo feedback in climate, *J. Clim.*, **17**, 1550–1568, 2004.

Hezel, P.J., Zhang, X., BItz, C.M., Kelly, B.P., and Massonnet, F.: Projected decline in spring snow depth on Arctic sea ice caused by progressively later autumn open ocean freeze-up this century, Geophys. Res. Lett., https://doi.org/10.1029/2012GL052794, 2012.

Holland, M. M. and Bitz, C. M.: Polar amplification of climate change in coupled models. *Clim. Dyn.* **21**, 221-232. Doi: 10.1007/s00382-003-0332-6, 2003.

Holland, M. M. & L. Landrum. The emergence and transient nature of Arctic amplification in coupled climate models, *Front. Earth Sci.*, **9**, https://doi.org/10.3389/feart.2021.719024, 2021.

Hunke, E. C., Lipscomb, W. H., Turner, A. K., Jeffery, N., and Elliot, S.: CICE: the Los Alamos Sea Ice Model Documentation and Software User's Manual Version 5.1, LA-CC-06-012., 2015.

Hurrell, J. W., Hack, J. J., Shea, D., Caron, J. M., and Rosinski, J.: A new sea surface temperature and sea ice boundary dataset for the Community Atmosphere Model. Journal of Climate, 21, 5145–5153, 2008.

Huwald H., Tremblay, L. B., and Blatter, H.: Reconciling different observational data sets from Surface Heat Budget of the Arctic Ocean (SHEBA) for model validation purposes. J Geophys Res 110:C05009. doi:10.1029/2003JC002221, 2005.

Jakobson, E., T. Vihma, T. Palo, L. Jakobson, H. Keernik, and J. Jaagus, J.: Validation of atmospheric reanalysis over the center Arctic Ocean. *Geophysical Res. Letters*, **39**, L10802, doi:10.1029/2012GL051591, 2012.

Kay, J. E. and Coauthors: The Community Earth System Model (CESM) Large Ensemble Project: a community resource for studying climate change in the presence of internal climate variability. *Bull. Am. Meteorol. Soc.* **96**, 1333–1349, 2015.

Keen, A., Blockley, E., Bailey, D. A., Boldingh Debernard, J., Bushuk, M., Delhaye, S., Docquier, D., Feltham, D., Massonnet, F., O'Farrell, S., Ponsoni, L., Rodriguez, J. M., Schroeder, D., Swart, N., Toyoda, T., Tsujino, H., Vancoppenolle, M., and Wyser, K.: An inter-comparison of the mass budget of the Arctic sea ice in CMIP6 models, The Cryosphere, 15, 951–982, https://doi.org/10.5194/tc-15-951-2021, 2021.

Kumar, A., Perlwitz, J., Eischeid, J., Quan, X., Xu, T., Zhang, T., Hoerling, M., Jha, B., and Wang, W.: Contribution of sea ice loss to Arctic amplification, *Geophys. Res. Lett.*, *37*, L21701, doi:10.1029/2010GL045022, 2010.

Kwok, R.: Arctic sea ice thickness, volume, and multiyear ice coverage: losses and coupled variability (1958-2018), *Environ. Res. Lett*, **13**, 105005, 2018.

Labe, Z., Magnusdottir, G., & Stern, H.: Variability of Arctic sea ice thickness using PIOMAS and the CESM large ensemble. *Journal of Climate*, *31*(8), 3233–3247. https://10.1175/ JCLI-D-17-0436.1, 2018a.

Labe, Z.M., Peings, Y and Magnusdottir, G.: Contributions of ice thickness to the atmospheric response from projected Arctic sea ice loss, *Geophys. Res. Letters*, DOI:10.1029/2018GL078158, 2018b.

Landrum, L. Scripts for figures and analysis for "Influences of changing sea ice and snow thicknesses on winter Arctic heat fluxes". Zenodo https://doi.org/10.5281/zenodo.5161076, 2021.

Lang, A., Yang, S. and Kaas, E.: Sea ice thickness and recent Arctic warming. *Geophys. Res. Lett.*, **44**, 409–418, https://doi.org/10.1002/2016GL071274, 2017.

Laxon, S. W., and Coauthors: CryoSat-2 estimates of Arctic sea ice thickness and volume. *Geophys. Res. Lett.*, **40**, 732–737, https://doi.org/10.1002/grl.50193, 2013.

Lindsay, R., M. Wensnahan, A. Schweiger, and J. Zhang: Evaluation of seven different atmospheric reanalysis products in the Arctic. *J. Climate*, **27**, 2588–2606, https://doi.org/10.1175/JCLI-D-13-00014.1, 2014.

Lindsay, R., and Schweiger, A.: Arctic sea ice thickness loss determined using subsurface, aircraft, and satellite observations. *The Cryosphere*, *9*(1), 269–283. doi:10.5194/tc-9-269-2015, 2015.

Massonnet, F., Vancoppenolle, M., Goosse, H. and Coauthors: Arctic sea-ice change tied to its mean state through thermodynamic processes. *Nature Clim Change* **8,** 599–603, https://doi.org/10.1038/s41558-018-0204-z, 2018.

Meinshausen, M., Smith, S. J., Calvin, K. and Coauthors: The RCP greenhouse gas concentrations and their extensions from 1765 to 2300. *Climatic Change* 109, 213 doi:10.1007/s10584-011-0156-z, 2011.

Parkinson, C. L., D. J. Cavalieri, P. Gloersen, H. J. Zwally, and J. C. Comiso, Arctic sea ice extents, areas, and trends, 1978–1996, *J. Geophys. Res.*, 104(C9), 20,837–20,856, doi:10.1029/1999JC900082, 1999.

Peings, Y., and G. Magnusdottir, G.: Response of the wintertime Northern Hemisphere atmospheric circulation to current and projected Arctic sea ice decline: A numerical study with CAM5. *Journal of Climate*, *27*(1), 244–264. https://10.1175/JCLI-D-13-00272.1, 2014.

Petty, A. A., Holland, M. M., Bailey, D. A. and Kurtz, N T.: Warm Arctic, increased winter sea ice growth? *Geophys. Res. Lett.*, **45** (23), 12,922-12,930, https://doi.org/10.1029/2018GL079223, 2018.

Pithan, F. and Mauritsen, T.: Arctic amplification dominated by temperature feedbacks in contemporary climate models. *Nat. Geosci.* **7**, 181–184, 2014.

Screen, J. A. and Simmonds, I.: The central role of diminishing sea-ice in recent Arctic temperature amplification. *Nature* **464**, 1334–1337, 2010.

Screen, J. A., Simmonds, I., Deser, C., and Tomas, R.: The atmospheric response to three decades of observed Arctic sea ice loss, *J. Clim.*, *26*(4), 1230–1248, doi:10.1175/JCLI-D-12-00063.1, 2013.

Screen, J. A. and Coauthors: Consistency and discrepancy in the atmospheric response to Arctic sea-ice loss across climate models. *Nat. Geoscience* **11**(3), 155–163, https://doi.org/10.1038/s41561-018-0059-y, 2018.

Serreze, M. C., Barrett, A. P., Stroeve, J. C., Kindig, D. N., and Holland, M. M.: The emergence of surface-based Arctic amplification, *Cryosphere*, *3*(1), 11–19, doi:10.5194/tc-3-11-2009, 2009.

Serreze, M. C., and Barry, R. G.: Processes and impacts of Arctic amplification: A research synthesis, *Global Planet. Change*, *77*(1), 85–96, doi:10.1016/j.gloplacha.2011.03.004, 2011.

Serreze, M. C., and Stroeve, J.: Arctic sea ice trends, variability and implications for seasonal ice forecasting. *Philosophical Transactions of the Royal Society of London A: Mathematical, Physical and Engineering Sciences*, *373*(2045), https://doi.org/10.1098/rsta.2014.0159, 2015.

Semtner, A. J.: A Model for the Thermodynamic Growth of Sea Ice in Numerical Investigations of Climate. *J. Phys. Oceanogr.* **6**, 379-389, 1976.

Simpson, I. R., Bacmeister, J., Neale, R. B., Hannay, C., Gettelman, A., Garcia, R. R., and coauthors: An evaluation of the large-scale atmospheric circulation and its variability in CESM2 and other CMIP models. *Journal of Geophysical Research: Atmospheres*, 125, e2020JD032835. https://doi.org/10.1029/2020JD032835, 2020.

Smith, D. M., Screen, J. A., Deser, C., Cohen, J., Fyfe, J. C., García-Serrano, J., Jung, T., Kattsov, V., Matei, D., Msadek, R., Peings, Y., Sigmond, M., Ukita, J., Yoon, J.-H. and Zhang, X.: The Polar Amplification Model Intercomparison Project (PAMIP) contribution to CMIP6: investigating the causes and consequences of polar amplification, *Geosci. Model Dev.*, **12**, 1139–1164, https://doi.org/10.5194/gmd-12-1139-2019, 2019.

Sun, L., Allured, D., Hoerling, M., Smith, L., Perlwitz, J., Murray, D. and Eischeid, J.: Drivers of 2016 record Arctic warmth assessed using climate simulations subjected to Factual and Counterfactual forcing. *Weather and Climate Extremes* **19**, doi:10.1016/j.wace.2017.11.001, 2018.

Sun, L., Deser, C., and Tomas, R. A.: Mechanisms of stratospheric and tropospheric circulation response to projected Arctic sea ice loss*. *Journal of Climate*, *28*, 7824–7845. https://doi.org/10.1175/JCLI-D-15-0169.1, 2015.

Sun, Lantao, Clara Deser, Isla Simpson and Michael Sigmond: Uncertainty in the winter tropospheric response to Arctic Sea ice loss: the role of stratospheric polar vortex internal variability, *Journal of Climate*, under review.

Vavrus, S.: The impact of cloud feedbacks on Arctic climate under greenhouse forcing, *J. Clim.*, 17, 603–615, 2004.

Wang, C., Graham, R. M., Wang, K., Gerland, S., and Granskog, M.: Comparison of ERA5 and ERA-Interim near-surface air temperature, snowfall and precipitation over Arctic sea ice: effects on sea ice thermodynamics and evolution. Cryosphere, 13, 1661-1679, https: //doi.org/10.5194/tc-13-1661-2019, 2019.

Webster, M. A., I. G. Rigor, S. V. Nghiem, N. T. Kurtz, S. L. Farrell, D. K. Perovich, M. Sturm,. Interdecadal changes in snow depth on Arctic sea ice. *J. Geophys. Res. Oceans* **119**, 5395–5406, 2014.

Webster, M., Gerland, S., Holland, M. *et al.* Snow in the changing sea-ice systems. *Nature Clim Change* **8,** 946–953. https://doi-org.cuucar.idm.oclc.org/10.1038/s41558-018-0286-7, 2018.

Webster, M. A., DuVivier, A. K., Holland, M. M., and Bailey, D. A.: Snow on Arctic Sea Ice in a Warming Climate as Simulated in CESM. J. Geophys. Res.: Oceans, 125, e2020JC016308. https://doi.org/10.1029/2020JC016308, 2020.

Zhang, J., and D. A. Rothrock: Modeling global sea ice with a thickness and enthalpy distribution model in generalized curvilinear coordinates. *Mon. Wea. Rev.*, **131**, 845–861, https://doi.org/10.1175/1520-0493(2003)131<0845:MGSIWA>2.0.CO;2, 2003.

Table 1. Conductive heat fluxes (Fcond) calculated with equation 2 for example sea ice thicknesses (SIT), snow thicknesses (h_s), and temperature gradients (ΔT).

SIT (m)	h_s (m)	ΔT (°K)	Fcond (W m^{-2})
2.0	0.1	40.	30.
2.0	0.02	40.	37.5
2.0	0.1	20.	15.
2.0	0.02	20.	18.75
0.5	0.1	40.	68.57
0.5	0.02	40.	126.32
0.5	0.1	20.	34.29
0.5	0.02	20.	63.16

Figure captions

Figure 1. Changes in ensemble mean February net surface heat flux (netSHF; a-d) and surface temperatures (TS; e-h) for CESM2 PAMIP (a-c, e-g) and AMIP (d, h). PAMIP differences are from an 1850 pre-industrial control run where both SSTs and SICs are specified at 1850 levels. Differences from the PI are shown for PAMIP experiments with present-day SSTs and SICs (pdSST-pdSIC; a,e); present-day SSTs and future SICs ("pdSST-futArcSIC; b, f), and future SSTs and SICs (futSST-futArcSIC; c, g). AMIP simulations are from a 10-member ensemble and differences shown are ensemble mean of the final decade (2005-2014) minus the first decade (1950-1959) of the simulations. The 98% SIC contour is shown in black.

Figure 2. CESM1-LE February area-averaged Arctic Ocean (a) surface temperatures, turbulent ocean-sea ice heat fluxes and conductive heat fluxes; (b) SIC, SIT and snow thicknesses (h_s); and (c) effective snow thickness (K_{ratio}*h_s), and effective total thicknesses (heff). Ensemble means are show in the solid lines, ensemble ranges in opaque polygons. Arctic Ocean region is shown in the map insert in the middle panel.

Figure 3. February decadal mean changes (from 1950-1959) in surface temperatures (a, d), conductive heat fluxes (b, e), and effective sea ice + snow thickness (heff; e, f) for the 2010s (a, b, c) and 2050s (d, e, f). The 98% SIC for each decade is shown by the thick black contour. Stippled areas in the effective thickness (heff) change figures (c, f) indicate regions where changes

in effective snow thickness (K_{ratio}*h_s) account for 40% or more of the changes in the total effective thickness (heff = SIT + K_{ratio}*h_s).

Figure 4. February decadal mean changes (from 1950-1959) in Arctic Amplification ($\Delta TAS/\Delta TAS_{global}$; a, e, i), net surface heat fluxes (b, f, j), sea ice contribution to surface heat fluxes (c, g, k), and ocean contributions to surface heat fluxes (d, h, l) for the 2010s (a, b, c, d), the 2050s (e, f, g, h) and the 2090s (i, j, k, l). The 98% SIC for each decade is shown by the thick black contour.

Figure 5. CESM1-LE area-averaged anomalies (from 1950-1959 ensemble mean) for sea ice and ocean contributions to net surface heat fluxes (left axis), and sea ice concentrations (right axis) for February (left column) and October (right column) Arctic Ocean (top), Kara (middle) and Barents (bottom) seas. Ensemble means are show in the solid lines, ensemble ranges in opaque polygons. Geographic areas are shown in inset at bottom.

Figure 6. CESM1-LE February area-averaged Arctic Ocean (a) mean conductive heat fluxes from the model output ("CESM1-LE"; dark blue) and calculated from mean ice and snow thicknesses ("MNthick"; light blue), and the ratio of MNthick to CESM1-LE (red) and (b) sea ice areas by thickness category as well as total sea ice area (dark blue). Ensemble means are show in the solid lines, ensemble ranges in opaque polygons. The solid black line in top panel indicates a MNthick:CESM1-LE conductive heat flux ratio of 0.75 for reference.

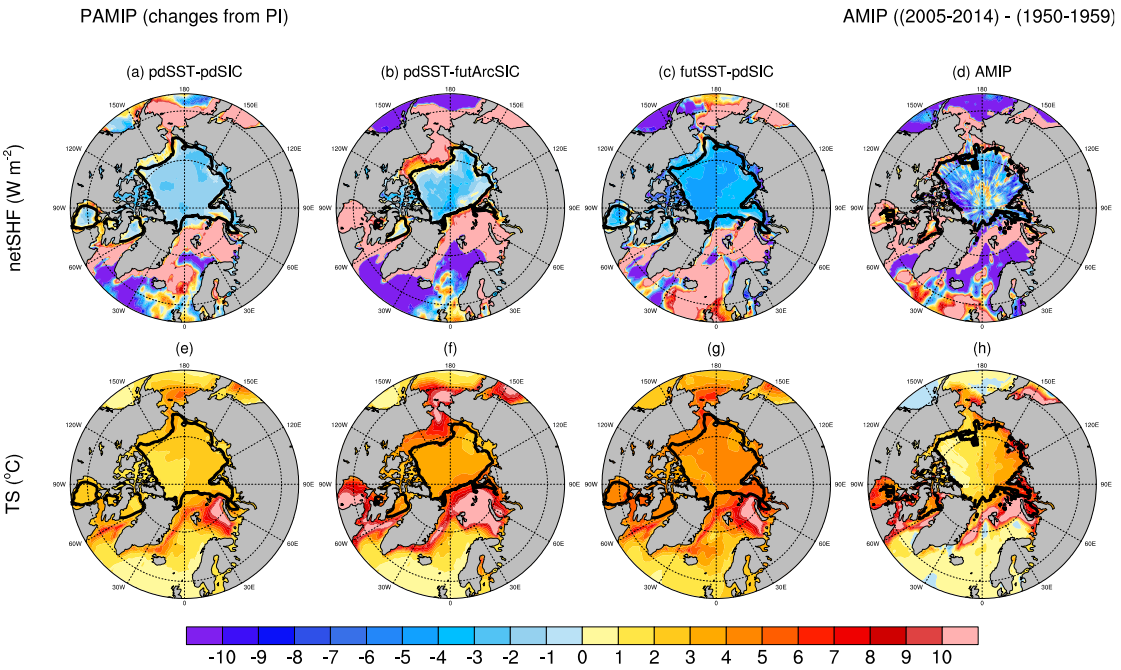
CESM2 (ens mean) FEB
PAMIP (changes from PI)
AMIP ((2005-2014) - (1950-1959)
(a) pdSST-pdSIC
(b) pdSST-futArcSIC
(c) futSST-pdSIC
(d) AMIP
(e)
(f)
(g)
(h)
netSHF (W m-2)
TS (°C)
-10 -9 -8 -7 -6 -5 -4 -3 -2 -1 0 1 2 3 4 5 6 7 8 9 10

515

Figure 1

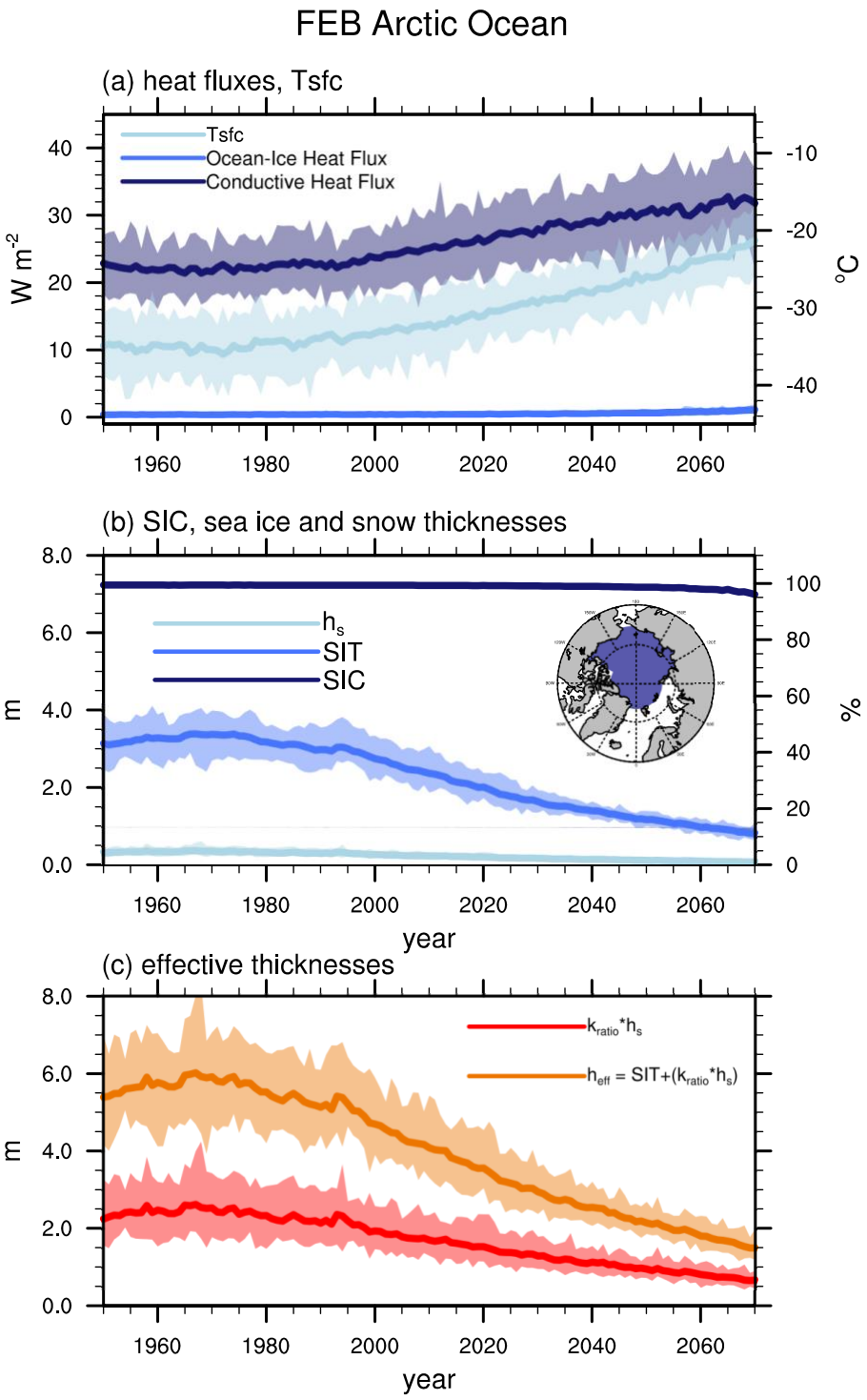
FEB Arctic Ocean
(a) heat fluxes, Tsfc
Tsfc
Ocean-Ice Heat Flux
Conductive Heat Flux
W m-2
°C
(b) SIC, sea ice and snow thicknesses
hs
SIT
SIC
m
%
year
(c) effective thicknesses
kratio*hs
heff = SIT+(kratio*hs)
m
year

Figure 2

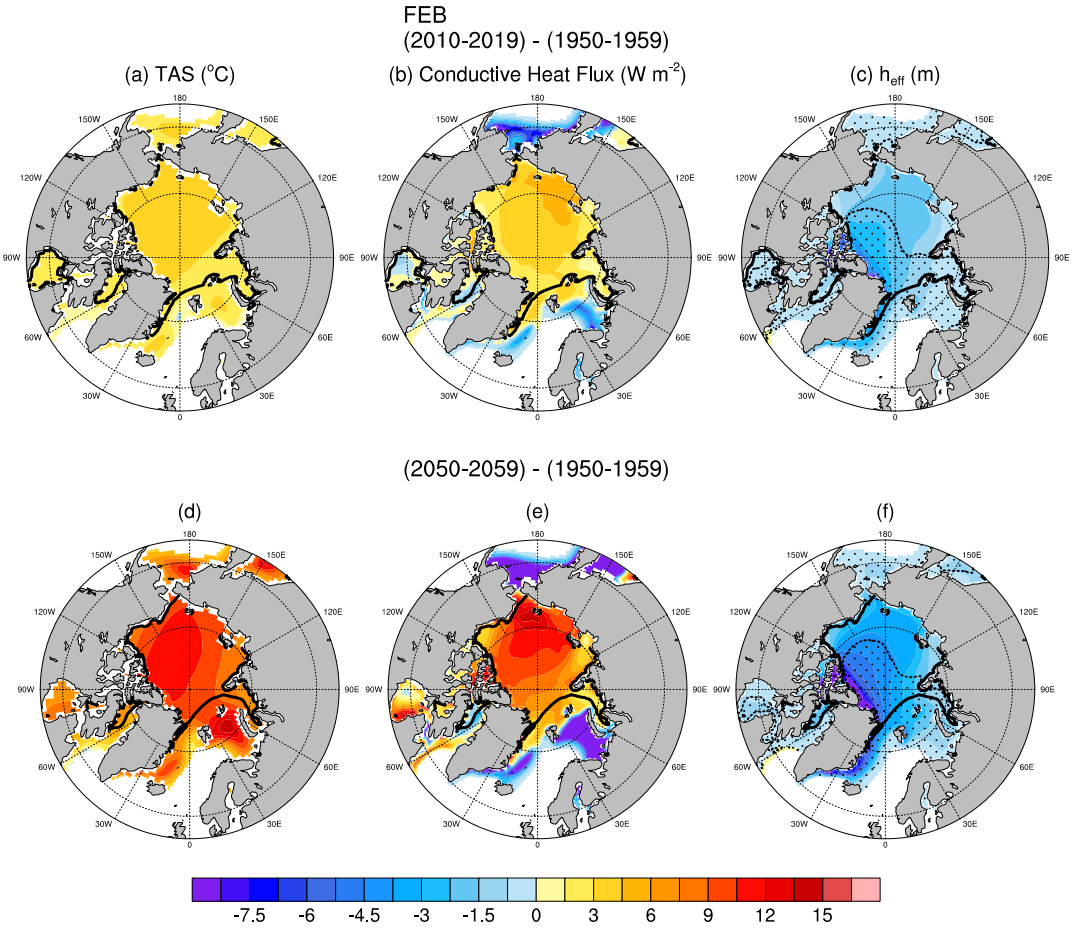
FEB
(2010-2019) - (1950-1959)
(a) TAS (°C)
(b) Conductive Heat Flux (W m-2)
(c) heff (m)
(2050-2059) - (1950-1959)
(d)
(e)
(f)
-7.5
-6
-4.5
-3
-1.5
0
3
6
9
12
15

520

Figure 3

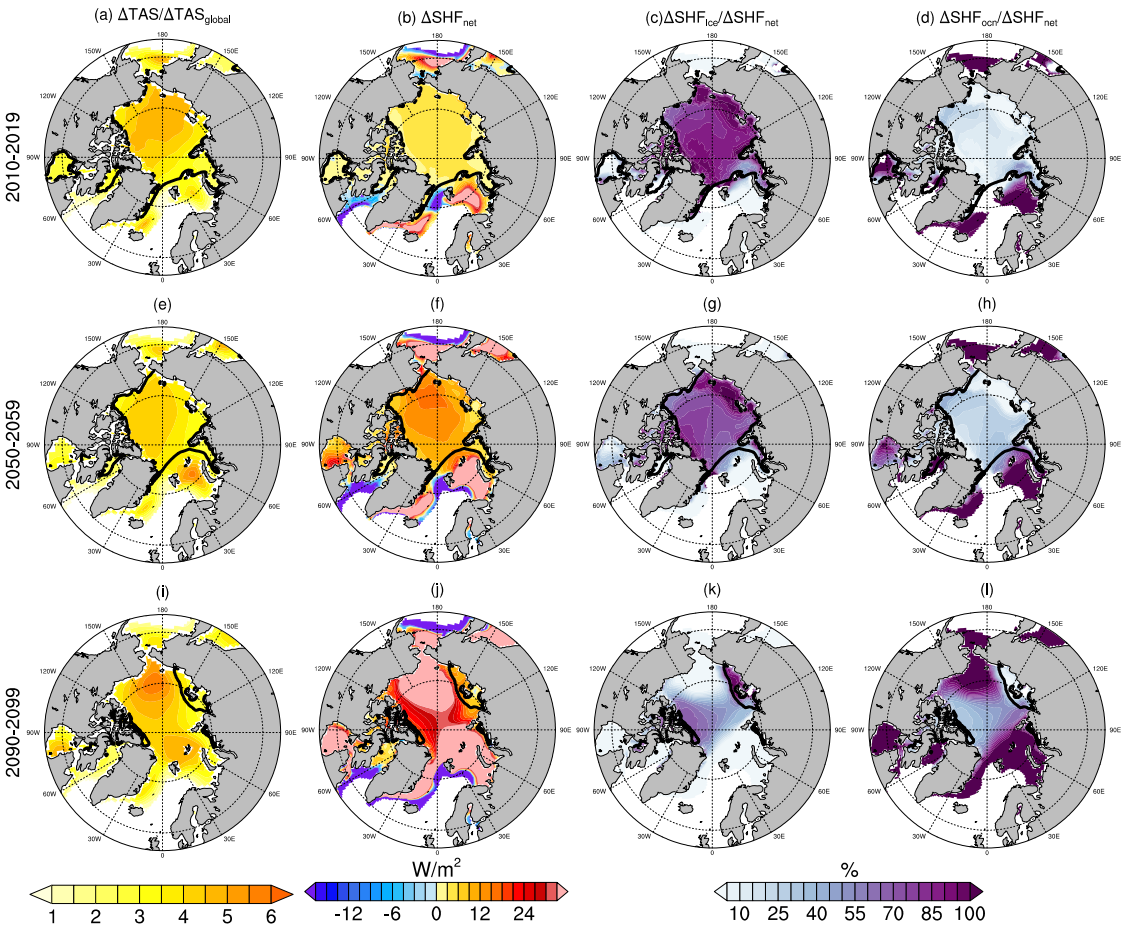
CESM1-LE
FEB
(a) ΔTAS/ΔTAS$_{global}$
(b) ΔSHF$_{net}$
(c)ΔSHF$_{Ice}$/ΔSHF$_{net}$
(d) ΔSHF$_{ocn}$/ΔSHF$_{net}$
2010-2019
2050-2059
2090-2099
(e)
(f)
(g)
(h)
(i)
(j)
(k)
(l)
1 2 3 4 5 6
W/m^2
-12 -6 0 12 24
%
10 25 40 55 70 85 100

Figure 4

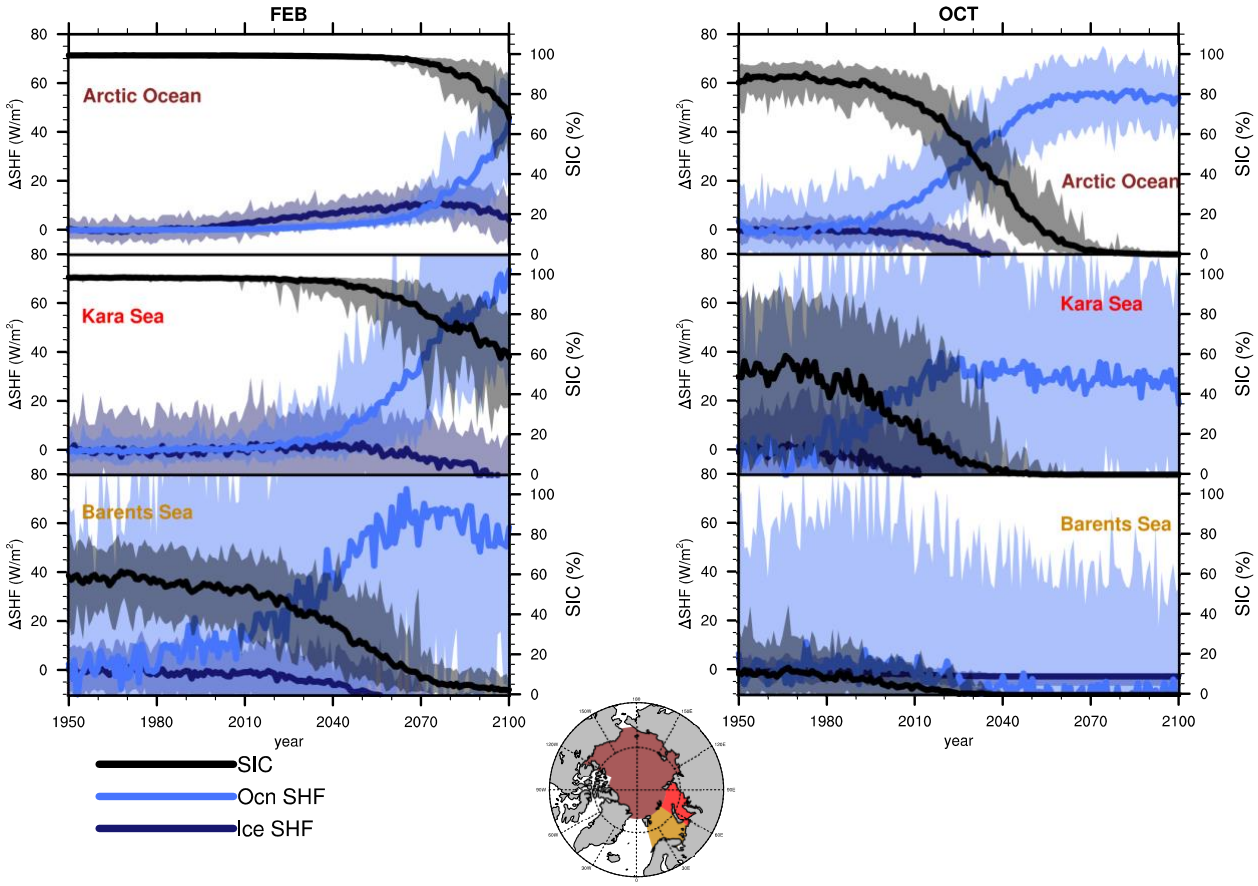
FEB
OCT
Arctic Ocean
Kara Sea
Barents Sea
ΔSHF (W/m²)
SIC (%)
year
1950
1980
2010
2040
2070
2100
SIC
Ocn SHF
Ice SHF

525 **Figure 5**

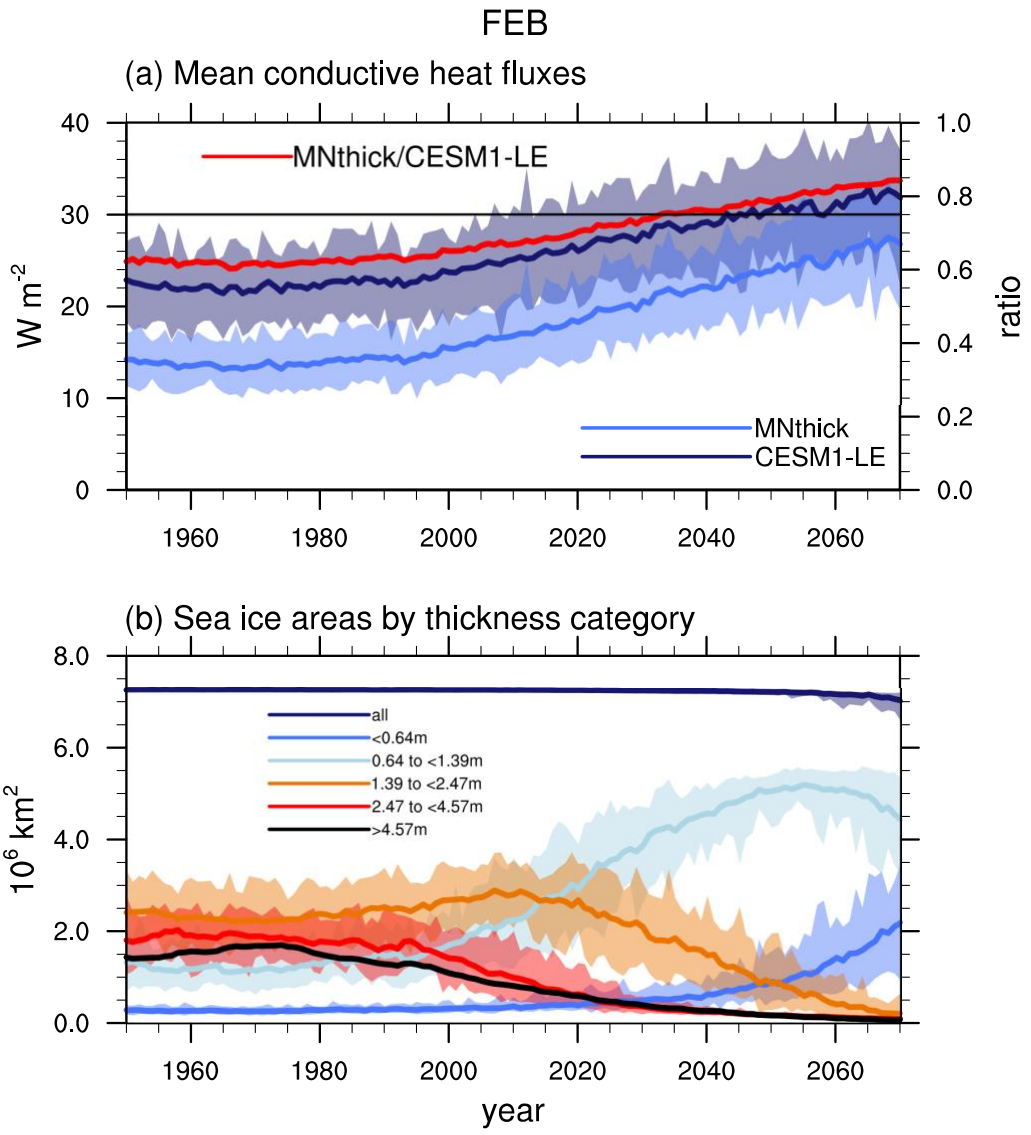
FEB
(a) Mean conductive heat fluxes
MNthick/CESM1-LE
MNthick
CESM1-LE
W m-2
ratio
40
30
20
10
0
1.0
0.8
0.6
0.4
0.2
0.0
1960
1980
2000
2020
2040
2060
(b) Sea ice areas by thickness category
all
<0.64m
0.64 to <1.39m
1.39 to <2.47m
2.47 to <4.57m
>4.57m
10^6 km^2
8.0
6.0
4.0
2.0
0.0
year

Figure 6